JGR Space Physics

RESEARCH ARTICLE
10.1029/2018JA026355

Long-Term Variations in Solar Wind Parameters, Magnetopause Location, and Geomagnetic Activity Over the Last Five Solar Cycles

A. A. Samsonov[1], Y. V. Bogdanova[2], G. Branduardi-Raymont[1], J. Safrankova[3], Z. Nemecek[3], and J.-S. Park[4]

[1]Mullard Space Science Laboratory, University College London, London, UK, [2]RAL Space, STFC Rutherford Appleton Laboratory, UK Research and Innovation, Oxford, UK, [3]Faculty of Mathematics and Physics, Charles University, Prague, Czech Republic, [4]Shandong Provincial Key Laboratory of Optical Astronomy and Solar-Terrestrial Environment, Institute of Space Sciences, Shandong University, Weihai, China

Key Points:
- Average annual magnetopause standoff distance increased by nearly 2 R_E from 1991 to 2009
- Solar wind dynamic pressure anticorrelates with sunspot number in cycles 20–21 and correlates in cycles 22–24
- The best correlation between annual solar wind dynamic pressure and sunspot number was found for 2- to 3-year delay

Correspondence to:
A. A. Samsonov,
a.samsonov@ucl.ac.uk

Citation:
Samsonov, A., Bogdanova, Y. V., Branduardi-Raymont, G., Safrankova, J., Nemecek, Z., & Park, J.-S. (2019). Long-term variations in solar wind parameters, magnetopause location, and geomagnetic activity over the last five solar cycles. *Journal of Geophysical Research: Space Physics*, *124*, 4049–4063. https://doi.org/10.1029/2018JA026355

Received 30 NOV 2018
Accepted 25 APR 2019
Accepted article online 30 APR 2019
Published online 6 JUN 2019

Abstract We use both solar wind observations and empirical magnetopause models to reconstruct time series of the magnetopause standoff distance for nearly five solar cycles. Since the average annual interplanetary magnetic field (IMF) B_z is about zero, and the annual IMF cone angle varies between 54.0° and 61.2°, the magnetopause standoff distance on this timescale depends mostly on the solar wind dynamic pressure. The annual IMF magnitude well correlates with the sunspot number (SSN) with a zero time lag, while the annual solar wind dynamic pressure (*Pdyn*) correlates reasonably well with the SSN but with 3-year time lag. At the same time, we find an anticorrelation between *Pdyn* and SSN in cycles 20–21 and a correlation in cycles 22–24 with 2-year time lag. Both the annual solar wind density and velocity well correlate with the dynamic pressure, but the correlation coefficient is higher for density than for velocity. The 11-year solar cycles in the dynamic pressure variations are superimposed by an increasing trend before 1991 and a decreasing trend between 1991 and 2009. The average annual solar wind dynamic pressure decreases by a factor of 3 from 1991 to 2009. Correspondingly, the predicted standoff distance in Lin et al.'s (2010, https://doi.org/10.1029/2009JA014235) magnetopause model increases from 9.7 R_E in 1991 to 11.6 R_E in 2009. The annual SSN, IMF magnitude, and magnetospheric geomagnetic activity indices display the same trends as the dynamic pressure. We calculate extreme solar wind parameters and magnetopause standoff distance in each year using daily values and find that both extremely small and large standoff distances during a solar cycle preferably occur at solar maximum rather than at solar minimum.

1. Introduction

Periodic variations of the coronal magnetic field (solar cycles) are synchronized with many processes in the geospace environment. Besides the well-known 11-year solar cycles, longer solar periodicities have also been revealed in the ground data. In particular, the studies of auroral records show variations with a mean period of about 80–90 years (Gleissberg, 1965; Link, 1962; Siscoe, 1980) often referred to as the Gleissberg cycle. The solar variations are transported to the Earth through the solar wind, solar energetic particles, and solar radiation. The 11-year periodicity has been observed in most solar wind parameters, such as the interplanetary magnetic field (IMF) magnitude (King, 1979), the IMF $|B_z|$ (Siscoe et al., 1978), and the helium content (Aellig et al., 2001; Neugebauer, 1981) almost from the start of the space era. A similar periodicity was found in the solar wind plasma parameters, for example, density and velocity (Dmitriev et al., 2009).

However, the cycles of solar wind parameters and indices of geomagnetic activity might not have the same phase or shape as the sunspot cycle (Feynman, 1982; Hirshberg, 1973). In particular, Echer et al. (2004) reported about an average 1-year time lag between the time series of the geomagnetic *aa* index and sunspot numbers (SSN) using correlation analysis for the period of 1868–2000. At the same time, the authors noted that the time lag varied during the time interval. Gonzalez et al. (1990) observed a dual-peak solar cycle distribution of intense geomagnetic storms, with first peak occurring at the late ascending phase of the cycle or at solar maximum and second peak at the early descending phase of the cycle. The solar phenomena responsible for geomagnetic storms are coronal mass ejections (CMEs) and corotating interaction regions

(CIRs). The occurrence rate of CMEs peaks during solar maximum, while the occurrence rate of CIRs peaks during the declining phase of the solar cycle (Borovsky & Denton, 2006, and references therein). Bothmer and the EU-INTAS-ESA Team (2004) noted that CIRs may play a role also during the rising phase. In general, however, the CME-driven storms mostly occur near solar maximum, and the CIR-driven storms mostly occur in the declining phase.

Several papers studied long-term variations in the solar wind velocity and the open solar magnetic flux by making reconstruction of the velocity from the geomagnetic indices (Lockwood et al., 2009; Rouillard et al., 2007). They mostly used the *aa* index because the time series for *aa* is longer than for other geomagnetic indices. According to Lockwood et al. (2009), the reconstructed annual solar wind velocity varied nearly from 300 to 550 km/s during the twentieth century. The averaged solar wind velocity and IMF magnitude obtained from in situ data between 1965 and 2010 were presented and discussed by Zerbo et al. (2013). This study also indicated significant variations in the solar wind speed which generally match the variations in the *aa* index. (Dmitriev et al., 2005, 2009) analyzed solar wind plasma and magnetic field properties during four solar cycles from 20th to 23rd. In particular, Dmitriev et al. (2009) obtained the periodicity and distribution functions for several dimensional and dimensionless parameters. They showed that the statistical distributions of both IMF magnitude and solar wind density are close to a lognormal distribution function, while the velocity distribution is different from a lognormal one. This reflects the observational fact that the relative dispersion of average solar wind velocity is smaller than the relative dispersion of IMF magnitude or solar wind density.

The last (24th) solar cycle has the lowest sunspot activity since the Dalton minimum (early 1800s). Janardhan et al. (2015) reported that the solar photospheric fields at high latitudes have been steadily declining since 1995. McComas et al. (2013) compared average solar wind parameters observed from the mid-1970s to the mid-1990s and from 2009 to the beginning of 2013. They showed a significant decrease in the proton temperature, mass and momentum fluxes, and IMF magnitude in the last solar cycle and noted that these results may have important implication for the solar wind interaction with planetary magnetospheres. Similar results were obtained by Zerbo and Richardson (2015) who noted that the solar wind magnetic field, speed, and density remained anomalously low from the 23rd solar minimum to the 24th solar maximum. The weak solar activity and small IMF result in decrease of the geomagnetic activity at the same time. Kilpua et al. (2014) examined the geomagnetic activity using *Dst* and *AE* indices, the solar wind conditions, and the occurrence rate of interplanetary coronal mass ejections during two periods, from 1995 to 1999 and from 2006 to 2012. They concluded that the geomagnetic activity was considerably weaker during the second time interval, in particular in terms of *Dst*, and related this mainly to a weaker southward IMF component.

The variations of solar wind parameters, such as the velocity and B_z magnitude, modulate the solar wind energy input into the magnetosphere through the variations of the reconnection rate at the dayside magnetopause. Besides, another consequence of variations in the solar wind parameters might be variable magnetospheric compression. Petrinec et al. (1991) used 10-year International Sun-Earth Explorer (ISEE) data from 1977 to 1987 to study variations of the magnetopause size and shape with the solar wind data. Surprisingly, they found that the solar wind dynamic pressure was the lowest values at solar maximum, in the 1979–1980 season, and the dynamic pressure had largest values, more than double the value in 1979–1980, at the following solar minimum. According to most magnetopause models, the magnetopause standoff distance depends both on the solar wind dynamic pressure and IMF B_z. Since there are no continuous observations at the dayside magnetopause, the variations of magnetopause position during a solar cycle may be difficult to detect directly using in situ observations. However, Petrinec et al. (1991) concluded that the average size of the magnetosphere varies significantly throughout the course of the solar cycle for both northward and southward IMF orientations. In agreement with the variations of the dynamic pressure, the standoff magnetopause distance was largest near solar maximum. Richardson et al. (2000) studied the same solar maximum of cycle 21 using solar wind data and geomagnetic *aa* index and showed both a temporal reduction in average solar wind speed and IMF magnitude and an associated depression in *aa* index in 1980. Dmitriev et al. (2005) also noted drops of the solar wind dynamic pressure and flux density near solar maxima, especially in cycles 20 and 21.

To our knowledge, the long-term variations in the magnetopause size have not been studied so far, except for the above-mentioned work of Petrinec et al. (1991) in which only a relatively short time interval was investigated. At present, in situ solar wind data referred to the bow shock nose are available in the OMNIWeb

database for almost five solar cycles. Besides, many empirical magnetopause models have been developed in order to predict the standoff distance as a function of the solar wind input parameters (Dmitriev et al., 2011; Kuznetsov & Suvorova, 1998; Lin et al., 2010; Petrinec & Russell, 1996; Pudovkin et al., 1998; Roelof & Sibeck, 1993; Shue et al., 1998). Despite some quantitative discrepancies in model predictions (Samsonov et al., 2016), they mostly use the same expressions connecting the solar wind dynamic pressure with the standoff distance. It is also known (and will be demonstrated again below) that the average IMF B_z on the timescale of months or years is approaching zero (see, e.g., Dmitriev et al., 2009); therefore, we believe that the dynamic pressure is the main factor which determines the long-term variations in the magnetopause size.

Recent studies have pointed out that during intervals with a nearly radial IMF orientation, the dayside magnetopause expands (Dušík et al., 2010; Grygorov et al., 2017; Jelínek et al., 2010; Merka et al., 2003; Park et al., 2016) due to a significant decrease in the total pressure in the magnetosheath (Samsonov et al., 2012; Suvorova et al., 2010). In some exceptional cases, such time intervals may last several hours, and this may shift the magnetopause position about 1–2 R_E outward (Samsonov et al., 2017). The magnetopause models have not taken into account this effect so far; nevertheless, we discuss the influence of quasi-radial IMF intervals on our results below.

The main motivation of this work is to investigate how the average magnetopause size has varied in the space era using OMNI data and empirical magnetopause models. We do not only limit our attention to variations in the solar wind dynamic pressure but also explore variations in the IMF B_z and $|B|$ and in the geomagnetic indices searching for similar long-term trends. In addition to the study of average annual values, we consider variations in the extreme annual solar wind values and the extreme standoff distance. We highlight several events when our method predicts the extreme standoff distance and discuss them.

During very strong magnetospheric compressions, geosynchronous orbits may partly leave the magnetosphere and cross the magnetosheath or solar wind (such events are called geosynchronous magnetopause crossings or GMCs). GMCs require sufficiently high dynamic pressures because the effects of negative IMF B_z are saturated (Suvorova et al., 2005). GMCs may cause a significant damage to the geosynchronous spacecraft; therefore, predictions of such events are an important space weather problem (Dmitriev et al., 2014; Dmitriev et al., 2016). In this work, we estimate the range of variations in the extreme annual magnetopause distance during the last five solar cycles using empirical magnetopause models.

The main reason of strong magnetospheric compression is a high solar wind dynamic pressure which is usually associated with a high solar wind speed. The intervals of high speed in the solar wind are associated both with CMEs and CIRs; however, an extremely high speed (e.g., $V_{SW} > 1,000$ km/s) is usually related to CMEs (Gopalswamy, 2006, 2008; Yashiro et al., 2004). Consequently, extremely strong magnetic storms (in terms of the *Dst* index) are mostly CME driven (Borovsky & Denton, 2006; Denton et al., 2006; Gosling et al., 1990). Strong storms sometimes result from the interaction between two successive CMEs or a CME and a high speed stream (Liu et al., 2015; Lugaz et al., 2017). Oh et al. (2007) concluded that CMEs (or more precisely magnetic clouds) are also the most dominant and strong driver of interplanetary shocks. We suggest below that strong CMEs or sequences of CMEs result in events with extremely strong magnetospheric compression.

Besides the solar wind velocity, the dynamic pressure depends also on the solar wind density, and both CMEs and CIRs are usually accompanied by a density increase. We discuss below the correlations between the annual density, velocity, and dynamic pressure.

The paper is organized as follows. In section 2, we show and discuss the average and extreme solar wind and magnetospheric parameters over the last five solar cycles. In section 3, we investigate events when the magnetosphere is extremely compressed. We close the paper with discussion and conclusions.

2. Solar Wind and Magnetospheric Cycles and Trends

We begin this study with the hourly average solar wind parameters from OMNI (omniweb.gsfc.nasa.gov) and find the daily average values. Later, we use these daily averages when finding maximal and minimal extreme values for each year (we call them *extreme annual values* below). On the next step, we calculate both the monthly and annual average values from the daily averages. The OMNI database contains solar wind parameters from 1964, but the data in 1964 and 1965 have many gaps; therefore, we consider only the time interval from 1966 to 2018. However, the OMNI data still contain a lot of data gaps before 1995 (Lockwood

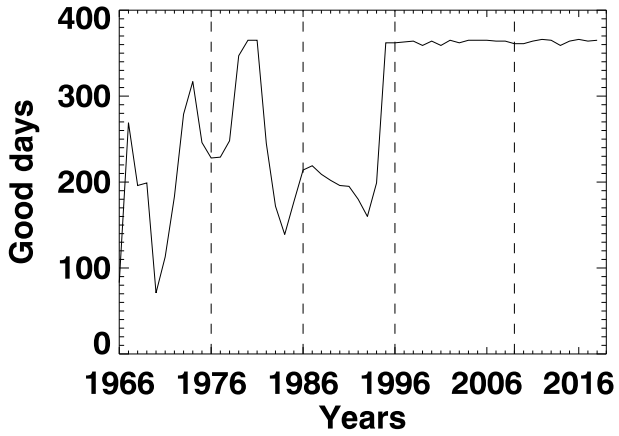

Figure 1. The number of days in each year which we have used for finding average annual values.

et al., 2019). We exclude daily averages from the processing if they contain less than 8-hourly average solar wind values, either in magnetic field or in plasma data. Figure 1 shows the number of "good" days, that is, the days which can be used to find the averages for each year. We have tried different minimum threshold conditions demanding from 5 to 12 hr of good data for each day and found that the averages are slightly changed only before 1995 and that this does not change the conclusions of the paper. Thus, the considered time interval covers completely three solar cycles (21–23) and almost completely the 20th and 24th cycles, so nearly five cycles in total.

For a given solar wind dynamic pressure and IMF, we calculate the magnetopause standoff distance using Shue et al.'s (S98) and Lin et al.'s (L10) magnetopause models. We use the magnetospheric *Dst* and *Kp* indices for illustration of the magnetospheric response to solar wind variations. The *Dst* index reflects the variations in the ring current, magnetopause current, and partly in the tail current (Burton et al., 1975). We will use $-Dst$ throughout the paper because increase in the geomagnetic activity actually means decrease in *Dst*. The *Kp* index indicates the level of overall magnetospheric disturbance.

Figure 2 shows the annual SSN, average and extreme IMF magnitude and B_z (we use GSM coordinates here and below), IMF cone angle (the angle between IMF vector and x axis, i.e., $acos(|B_x|/|B|)$), solar wind dynamic pressure *Pdyn* and velocity, magnetopause standoff distance, and $-Dst$ index. We discuss first the extreme annual solar wind values shown by red and blue lines in Figure 2. The maximum $|B|$, maximum and minimum B_z, maximum dynamic pressure, and finally maximum solar wind velocity in general display the 11-year cycle similar to the SSN, although with large fluctuations. The two exceptions are cycle 20 when both the maximum $|B|$ and maximum *Pdyn* (and V) do not reveal any increase near solar maximum and cycle 21 in which a great increase of maximum *Pdyn* occurs at the beginning of the cycle, in 1976–1977. The average annual dynamic pressure (shown in both Figures 2 and 4) in cycles 20–21 exhibits the same trends as the maximum *Pdyn*. Considering these two cycles, Crooker and Gringauz (1993) concluded that the dynamic pressure anticorrelates with the SSN, but we do not confirm this conclusion when analyzing the whole five-cycle interval.

Since the extreme values in Figure 2 are obtained from daily averages (one extreme value for each year), we believe that they probably correspond to the strongest CMEs in each year reaching the Earth. Note that the date with extreme conditions for one parameter (e.g., for $|B|$) usually does not coincide with the date with extreme conditions for another parameter (e.g., *Pdyn*). However, the solar wind conditions for a whole day whether with a strong dynamic pressure, for example, on average higher than 10 nPa, or with a high negative B_z, for example, about −10 nT or lower, result in significant magnetospheric disturbances, possibly commencing magnetic storms.

Increase in the solar wind dynamic pressure results in decrease in the minimum magnetopause standoff distance as shown by blue lines on the seventh panel from the top of Figure 2. Both S98 and L10 models predict the smallest daily standoff distance in the middle of the 22nd cycle, in 1991, when the standoff distance decreased to 5.9 R_E (see Table 3 below). Interestingly, the variations in the maximum standoff distance also roughly follow the solar cycles. The peaks in the maximum standoff distance which correspond to the

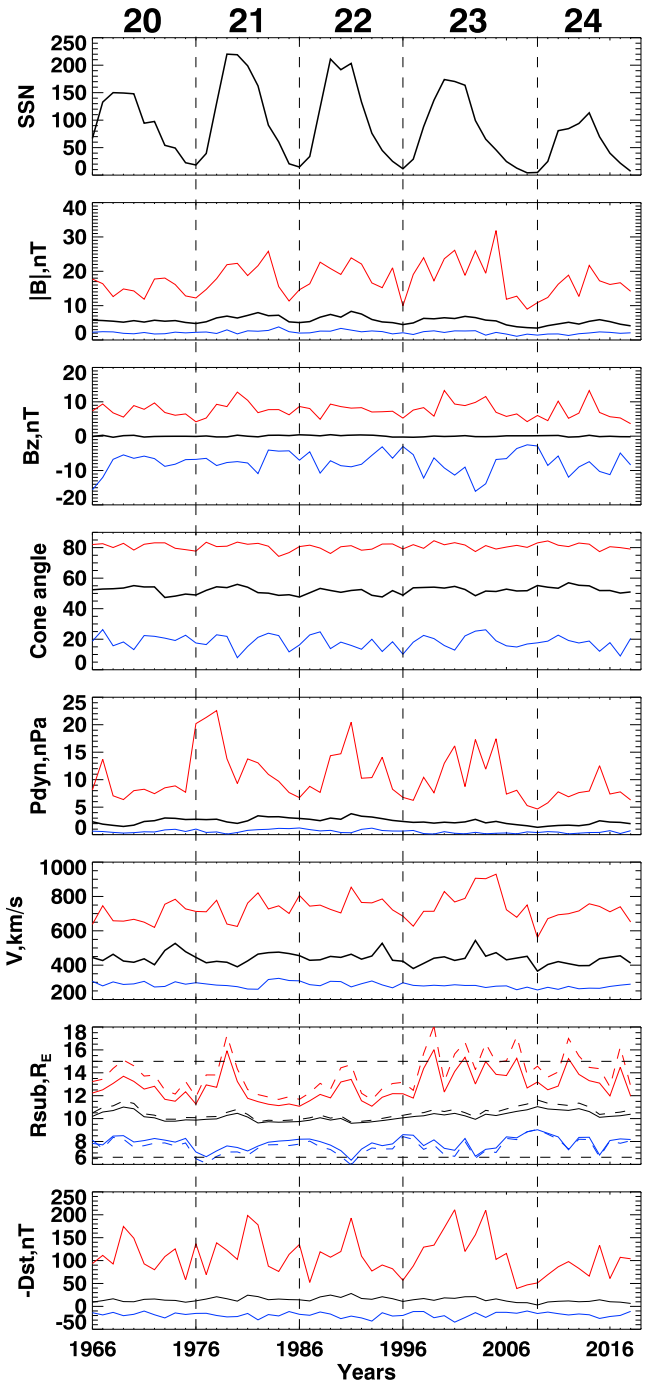

Figure 2. The sunspot numbers (average daily number for each year), average and extreme interplanetary magnetic field (IMF) magnitude and B_z, IMF cone angle (the angle between IMF vector and x axis), solar wind dynamic pressure and velocity, magnetopause standoff distance (solid lines for Shue et al.'s model and dashed lines for Lin et al.'s model), and geomagnetic $-Dst$ index. Annual average values are shown by black; daily maximal and minimal values for each year are shown by red and blue. Vertical lines separate solar cycles as indicated by numbers at the top. SSN = sunspot number.

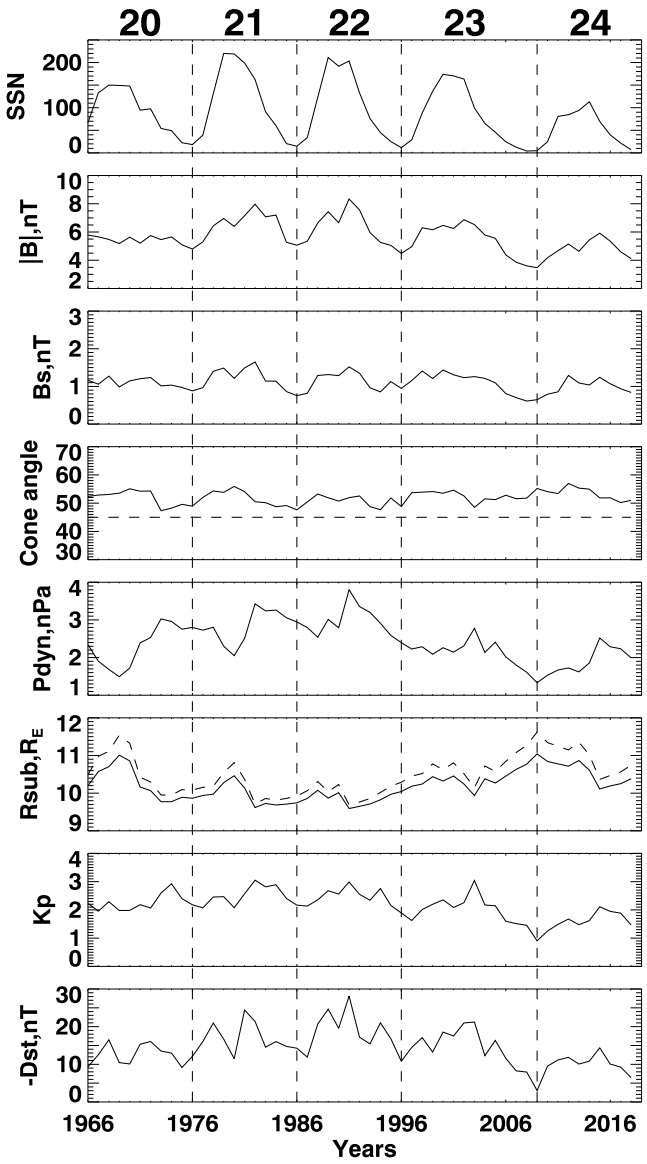

Figure 3. Expanded view of the annual average values from Figure 2 (except for B_s and *Kp*). From the top, the sunspot numbers, interplanetary magnetic field magnitude, and average southward component B_s, interplanetary magnetic field cone angle, solar wind dynamic pressure, magnetopause standoff distance (solid lines for Shue et al.'s model and dashed lines for Lin et al.'s model), *Kp* and *Dst* indices. Vertical lines separate solar cycles as indicated by numbers at the top. SSN = sunspot number.

deepest minima of the dynamic pressure are located mainly in the middle of solar cycles, although the correlation between maximum *Rsub* and SSN is poor. In other words, the probability of getting an extremely small dynamic pressure seems to be higher near solar maximum than near solar minimum too. This is also the case for the extremely large dynamic pressure. The correlation between the maximum annual dynamic pressure and the annual SSN is statistically significant with the coefficient of 0.364.

Comparing the results of S98 (solid) and L10 (dashed) magnetopause models, we conclude that both models predict qualitatively very similar variations (since they are determined by dynamic pressure in both cases), but the L10 model usually predicts slightly larger maximum or smaller minimum standoff distance. The reason for this is that the L10 model implies a stronger dependence of the standoff distance on the dynamic pressure ($R_{S98} \sim Pdyn^{-0.15}$, while $R_{L10} \sim (Pdyn + Pm)^{-0.19}$, here *Pm* is magnetic pressure). The maximum *Dst* index also displays the 11-year cycle as expected.

Table 1
Pearson Correlation Coefficients for Annual Sunspot Numbers, Solar Wind Parameters, Magnetopause Distance Calculated by L10 Model, and Magnetospheric Indices for a Zero Time Lag Between All Parameters

Parameter	SSN	$\|B\|$	*Bs*	θ	*N*	*V*	*Pdyn*	*Rsub*	*Kp*	*Dst*
SSN	1.000	0.748	0.784	0.301	N	N	N	N	0.435	−0.611
$\|B\|$	0.748	1.000	0.833	N	0.339	0.321	0.665	−0.588	0.836	−0.808
Bs	0.784	0.833	1.000	N	N	N	0.340	−0.301	0.584	−0.714
θ	0.301	N	N	1.000	−0.512	−0.608	−0.718	0.748	−0.514	N
N	N	0.339	N	−0.512	1.000	N	0.763	−0.792	0.359	−0.371
V	N	0.321	N	−0.608	N	1.000	0.553	−0.543	0.715	−0.346
Pdyn	N	0.665	0.340	−0.718	0.763	0.553	1.000	−0.976	0.828	-0.628
Rsub	N	−0.588	−0.301	0.748	−0.792	−0.543	−0.976	1.000	-0.793	0.582
Kp	0.435	0.836	0.584	−0.514	0.359	0.715	0.828	−0.793	1.000	−0.744
Dst	−0.611	−0.808	−0.714	N	−0.371	−0.346	−0.628	0.582	−0.744	1.000

Note. Letter N instead of some correlation coefficients indicates that the correlation between these parameters is not statistically significant. The correlation between SSN and *Pdyn* (*Rsub*) increases for a nonzero time lag (see explanation in text and Figure 4 below). All correlation coefficients for *Dst* are negative because *Dst* becomes stronger negative for more disturbed magnetospheric conditions. SSN = sunspot number.

After emphasizing the extreme solar wind parameters in Figure 2, we now consider the solar cycles and long-term trends in the average annual values. Figure 3 shows the annual SSN, IMF magnitude and average southward IMF, IMF cone angle, solar wind dynamic pressure, magnetopause standoff distance, and *Kp* and −*Dst* indices. The average southward component B_s has been obtained from hourly B_z such that $B_s = 0$ for $B_z > 0$ and $B_s = -B_z$ for $B_z < 0$. Both the average $|B|$ and B_s clearly vary with the 11-year periodicity, except may be during the twentieth cycle. Note that the number of days with data gaps in the twentieth cycle is larger than in the following cycles which might explain the different behaviors of the average parameters in this cycle. At the same time, magnetospheric indices in the twentieth cycle also do not clearly match the solar cycle variations as they usually do; therefore, the reason of unexpected variations in solar wind parameters in this cycle may be physical and is related to solar wind formation near the Sun.

According to Figure 3, the annual dynamic pressure exhibits slight correlation with the SSN (see discussion below), and even its annual plot displays several spikes in the whole five-cycle interval. We suggest that the spikes of *Pdyn* are related to strong CMEs or to pairs of CME-CME and CIR-CME (Lugaz et al., 2017), which usually concentrate near solar maximum and in the declining phase.

We quantify the correlations in Figure 3 by finding the Pearson correlation coefficients (Press et al., 1992) presented in Table 1. We show only the correlation coefficients for which p values < 0.05; that is, the correlation is statistically significant. The table demonstrates that the SSN well correlates with the IMF (the correlation coefficient r is 0.75 for $|B|$ and 0.78 for B_s) but does not correlate with both the solar wind density and velocity (and correspondingly with the dynamic pressure). The IMF cone angle weakly correlates with the SSN ($r = 0.30$), does not correlate with the IMF magnitude and B_s, but correlates reasonably well with the density (r =-0.51) and velocity (r =-0.61). The density and velocity do not correlate with each other but both correlate with the dynamic pressure, and the correlation coefficient is higher for density (r =0.76) than for velocity ($r = 0.55$). The magnetopause distance calculated by the L10 model anticorrelates extremely well with the dynamic pressure as expected. It is interesting to note that *Kp* better correlates with *Pdyn* and *V*, and *Dst* better correlates with *Bs*; however, both indices correlate well with $|B|$. As a result, the magnetopause distance is also better correlated with *Kp* ($r = -0.79$) than with *Dst* ($r = 0.58$). Finally, *Dst* better correlates with SSN ($r = -0.61$) than *Kp* ($r = 0.43$).

Previous studies showed (Luhmann et al., 2009) that high speed solar wind streams mostly occur in the declining phases of solar cycles; therefore, we have correlated the SSN and *Pdyn* with variable time lag from 1 to 11 years. Indeed, the correlation coefficient between the two parameters significantly increases: we obtain maximum correlation coefficient of 0.57 for the whole time series taking 3-year time lag and 0.68 for only the last three cycles taking 2-year time lag. This agrees with previous results; for example, Köhnlein (1996) obtained a 2-year time lag between the SSN and solar wind velocity. Contrary to the correlation for 0-year time lag, the correlations coefficients for 1- to 4-year time lags correspond to p values less than 0.05; that is,

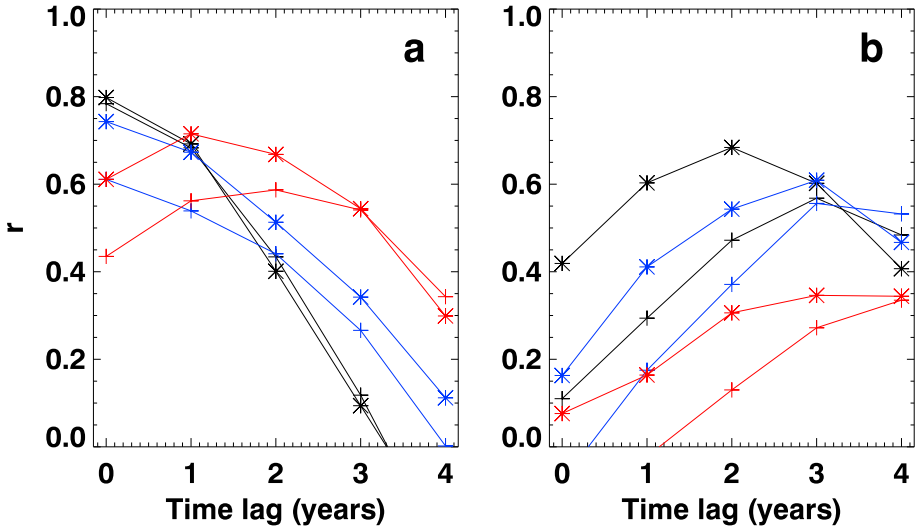

Figure 4. (a) The correlation coefficients between sunspot number and *Bs* (black), *Dst* (blue), and *Kp* (red) as a function of time lag for five (plus signs) and three (stars) solar cycles. (b) The correlation coefficients between sunspot number and *Pdyn* (black), *V* (blue), and *N* (red). Most correlations with coefficients below 0.3 are not statistically significant.

they are statistically significant. However, Crooker and Gringauz (1993) and Dmitriev et al. (2005) concluded that the dynamic pressure anticorrelates with the SSN analyzing mostly variations in cycles 20–21. If we consider separately the time interval between 1966 and 1986, we also find the anticorrelation between SSN and *Pdyn* with the coefficient of −0.51 (for zero time lag). Although this interval contains only 21 annual values, the correlation is statistically significant.

Since the correlations between the SSN and geomagnetic indices may also increase if taking into account a time lag (Echer et al., 2004), we calculate the correlations between the annual SSN and *Bs*, *Kp*, and *Dst* for variable time lags from 0 to 4 years. As we note above, the correlation between SSN and *Pdyn* is higher for the three last solar cycles than for the whole 53-year interval; therefore, we provide the coefficients for both the last five and three cycles. Figure 4 shows the results of calculations. The left panel shows the correlation coefficients for *Bs*, *Dst*, and *Kp*, while the right panel shows the coefficients for *Pdyn*, *V*, and *N*.

The correlation coefficients between SSN and *Bs* and SSN and *Dst* are highest for a 0-year time lag. The correlation between SSN and *Kp* is highest for 2-year time lag (for five cylces) and for 1-year time lag (for three cycles). As mentioned above, the correlation between SSN and *Pdyn* is highest for 2- to 3-year time lag depending on the time interval. The correlation coefficient between SSN and *V* peaks for 3-year time lag in both cases. The density correlation with the solar activity is significantly worse than with other solar wind parameters. In fact, the only statistically significant correlation (according to our criterion) has been obtained for 4-year time lag and five solar cycles interval. In this case, the correlation coefficient grows up to only 0.33.

Considering the whole 53-year interval in Figure 3, we note that the dynamic pressure increases until 1991 (except for the local minima in 1980 and 1990) and then follows a decreasing trend between 1991 and 2009. It increases again in the present cycle untill 2015. The average annual values vary significantly, from 3.80 nPa in 1991 to 1.33 nPa in 2009, that is, by a factor of 3. Respectively, the average magnetopause standoff distance varies between 9.59 R_E for the S98 model (9.68 R_E for the L10 model) in 1991 and 11.04 R_E for the S98 model (11.62 R_E for the L10 model) in 2009. Thus, the magnetopause models predict a 1.5–2 R_E variation in the standoff distance in the 17-year interval from the maximum of the 22nd to the minimum between the 23rd and 24th cycles.

In fact, the same decreasing trend after 1991 occurs for the other parameters in Figure 3, that is, for the SSN, |*B*|, and *Bs*. At the same time the *Dst* index increases (−*Dst* decreases) which may indicate both decrease in the average ring current and reduction in the magnetospheric compression (see discussion in section 4). To emphasize this trend, we draw the average solar wind and magnetospheric parameters for each solar cycle

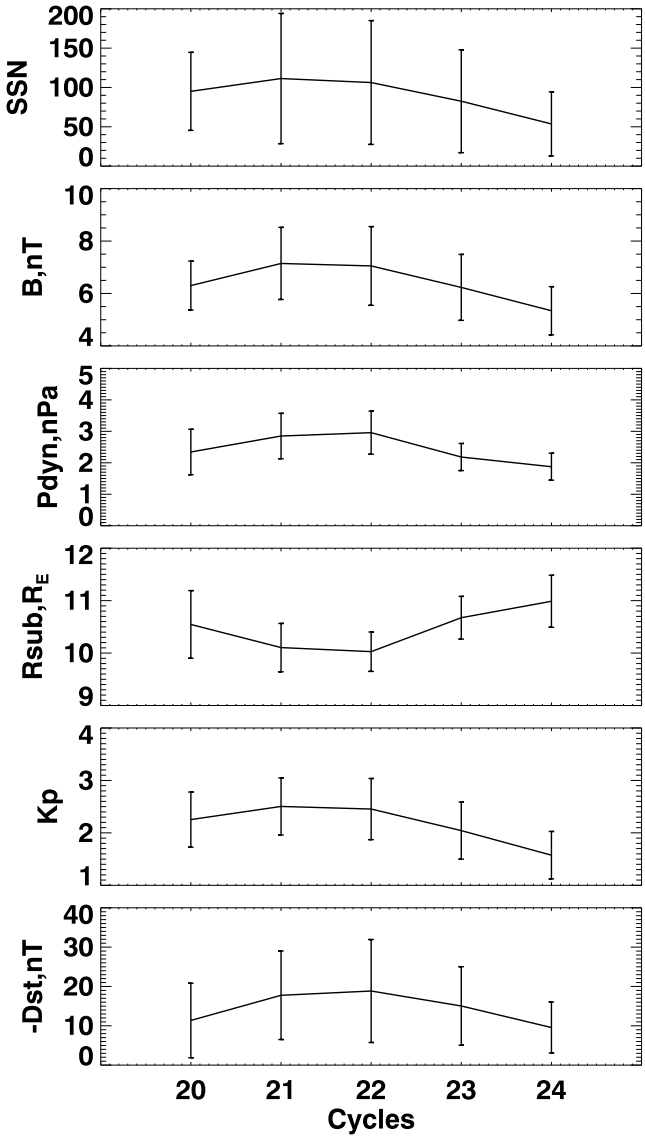

Figure 5. The sunspot numbers, interplanetary magnetic field magnitude, solar wind dynamic pressure, magnetopause standoff distance in the L10 model, and *Kp* and *Dst* indices averaged for each solar cycle. The error bars indicate standard deviations obtained from monthly values. SSN = sunspot number.

in Figure 5. In general, the trends for all of the parameters are very similar, taking into account that the variations of *Rsub* are reversed to *Pdyn*. Both the average SSN and $|B|$ have a maximum in the 21st cycle, while the solar wind dynamic pressure reaches its maximum in the 22nd cycle. However, the differences for all these parameters between the 21st and 22nd cycles are insignificant being smaller than the standard deviations. *Kp* has the maximum in the 21st cycle and *Dst* in the 22nd cycle, but *Kp* in the 21st cycle is only 0.5% higher than in the 22nd cycle.

We quantify the differences between cycles 22 and 24 in Table 2. As follows from the table, the average *Pdyn* and *Kp* decrease by 37% and 36%, respectively, between cycles 22 and 24, and *Rsub* increases from 10.0 to 11.0 R_E, that is, by 10%. If we compare the years 1991 and 2009, *Pdyn* and *Kp* decrease by 65% and 70% respectively, while *Rsub* increases by 20%. In particular, the values of *Rsub* according to the L10 model in 1991 and 2009 are 9.68 and 11.62 R_E, respectively. Note that the *Rsub* in the L10 model varies with *Pdyn* according to a power law index of only −0.19; however, the annual difference in the magnetopause position of about 2 R_E is significant and should be taken into account when preparing for the future space missions (as discussed in section 4).

Table 2
Comparison of Average Solar Wind and Magnetospheric Parameters in Cycles 22 and 24

Cycle (year)	SSN	$\lvert B\rvert$,nT	*Pdyn*,nPa	*Rsub*, R_E	*Kp*
$< N_{22} >$	106.3	7.0	2.96	10.0	2.45
$< N_{24} >$	53.6	5.3	1.87	11.0	1.57
$< N_{24} > / < N_{22} >$	0.50	0.76	0.63	1.10	0.64
N_{09}/N_{91}	0.024	0.42	0.35	1.20	0.30

Note. The magnetopause standoff distance is calculated by the L10 model. $< N_{22} >$ and $< N_{24} >$ are the average values for corresponding cycles; N_{09} and N_{91} are the average annual values in 2009 (minimum between 23rd and 24th cycles) and 1991 (maximum of 24th cycle), respectively. The bottom two rows are dimensionless. SSN = sunspot number.

3. Extreme Daily Magnetopause Distance

We further study the extreme solar wind conditions and identify the dates when the predicted magnetopause standoff distance is very small. We use the minimum daily average values shown by blue line in Figure 2. We take the L10 model which probably gives more realistic results for extreme solar wind and magnetospheric conditions (Dmitriev et al., 2016). Table 3 shows the dates and daily parameters for the events for which the model predicts the daily magnetopause distance to be less than 6.62 R_E, that is, GMCs. We can find only three such days probably because (1) the days with extreme solar wind conditions in the 20th and 21st cycles have large data gaps and (2) the condition for daily average *Rsub* <6.62 R_E is very restrictive. The average dynamic pressure is high, larger than 14 nPa, in all events, as expected. Moreover, the IMF B_z is strongly negative, which is the second reason for the decreasing of the magnetopause standoff distance. The daily dynamic pressures and B_z in these events match the necessary conditions for GMCs in Suvorova et al. (2005).

The last two events in Table 3 are classified as CME related in the ACE Richardson and Cane catalogue (www.srl.caltech.edu/ACE/ASC/DATA/level3/icmetable2.htm) and, moreover, are associated with the subsequent CMEs, suggesting that possibly complex and interacting CMEs are causing the closest standoff distance. The first event in 1991 seems to be also associated with a solar flare observed on 4 June and possibly CME related (Rank et al., 2001). The major magnetic storm of 4–5 June 1991 was studied by Garner et al. (2004). All the events have minimum *Dst* below −100 nT, therefore may be classified as magnetic storms, and *Kp* is 5.7 or higher.

We used 1-min averaged magnetic field data obtained from geosynchronous spacecraft GOES 8-13 and 15 to identify the GMC events with negative B_z. Only intervals lasting more than 5 min have been selected, and several events in 1 day have been classified as one event. Figure 6 reproduces the minimum annual magnetopause standoff distance for the L10 model shown in Figure 2 superimposed by the histogram with the number of days in each year when GOES observed negative B_z on the dayside (0600–1800 MLT). The last two events in Table 3 are also included in this statistics.

The histogram covers the interval from 1996 to 2017, but the GMCs were observed only around the maximum of the 23rd cycle, from 1999 to 2006, and in the 24th cycle from 2011 to 2014. Most of the crossings occur in 2000, 2001, and 2003, when the model predicts drops in the minimal standoff distance. In general, the anticorrelation between red and blue lines in Figure 6 seems to be good taking into account that the blue line reflects only minimum average magnetopause distance in 1 day, for example, in one event, for each

Table 3
The Dates With Daily Minimal Magnetopause Distance According to the L10 Model, the Daily Averages of Pdyn, B_z, and Rsub, Average and Minimal Dst, and Average Kp

Date	*Pdyn*, nPa	B_z, nT	*Rsub*, R_E	*Dst*	Dst_{min}	*Kp*
5 Jun 1991	20	−8.8	5.9	−147	−223	7.8
31 Mar 2001	14	−6.3	6.6	−211	−387	7.6
29 May 2003	17	−4.3	6.5	−46	−144	5.7

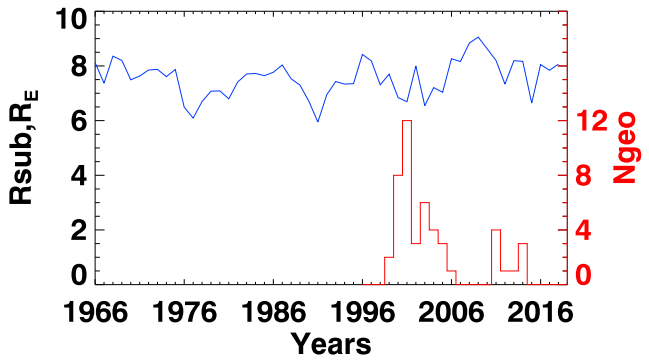

Figure 6. The annual minimal (blue) magnetopause standoff distance in the L10 model (the same as in Figure 2) and the number of days with negative B_z at geosynchronous orbit (red).

year. On the other hand, the red line may miss some GMC events if there were no GOES measurements at the particular time in the dayside region or GMCs were for positive B_z.

4. Discussion and Conclusions

This work investigates variations in the average magnetopause standoff distance from 1966 to 2018 using OMNI data and empirical magnetopause models. According to most empirical models, the standoff distance depends on the solar wind dynamic pressure and IMF B_z (e.g., Shue et al., 1998), but in addition to these two parameters, it may also depend on the solar wind magnetic pressure (Lin et al., 2010). Other parameters, such as the solar wind velocity (in addition to the dynamic pressure) or ionospheric conductivity, may control the magnetospheric compression too (Němeček et al., 2016), but their influence is not yet firmly established. The ring current may also control the magnetopause standoff distance during geomagnetically disturbed conditions, especially in the main phase of magnetic storms (Dmitriev et al., 2016). Moreover, recent studies show that the magnetosphere may significantly expand during intervals with nearly radial IMF (Dušík et al., 2010; Grygorov et al., 2017; Park et al., 2016; Suvorova et al., 2010; Suvorova & Dmitriev, 2015); however, this effect has not been incorporated in empirical models so far.

We use annual average and extreme solar wind and magnetospheric parameters in this work. On such a long timescale, the average IMF B_z approaches zero. The annual IMF cone angle varies in a narrow interval between 54.0° and 61.2° with the average of 57.6°. Since a quasi-radial IMF orientation usually means small cone angles, for example, less than or equal to 30° (Dušík et al., 2010), we think that quasi-radial intervals do not influence significantly our predictions of the magnetopause standoff distance on the annual timescale. As a result, the annual standoff distance depends mainly on the solar wind dynamic pressure. However, the power law indices of this dependence differ between the empirical models. For this reason, we have compared predictions of the two models, S98 and L10. The second model predicts stronger variations with *Pdyn* and possibly better corresponds to observations even for disturbed magnetospheric conditions (Samsonov et al., 2016; Suvorova & Dmitriev, 2015).

We have calculated both the annual average standoff distance and extreme distances for each year. The extreme distances have been defined as minimum and maximum daily values. Both the minimum and maximum standoff distances vary with solar cycles in such a way that not only very compressed but also expanded subsolar magnetosphere can be observed near solar maximum, rather than just near solar minimum. The annual IMF magnitude (IMF B_z) correlates with SSN with the correlation coefficients 0.75 (0.78) and a zero time lag. The annual average solar wind dynamic pressure correlates with the SSN with a coefficient of 0.57 if taking into account a time lag between *Pdyn* and SSN. We obtain a time lag of 3 years for the whole 53-year time interval. Considering only the three last cycles increases the correlation coefficient to 0.68 and gives a time lag of 2 years. The solar wind density poorly correlates with the SSN; the only statistically significant correlation occurs for a 4-year time lag, and the correlation coefficient grows up to only 0.33. The solar wind velocity correlates with the SSN better than the density, and the correlation coefficient is equal to 0.56 (0.61 for three cycles) for a time lag of 3 years. Both the density and velocity do not correlate with the IMF B_z for a zero time lag, very poorly correlate with the IMF $|B|$, but significantly better anticorrelate with the IMF cone angle. The correlation coefficient between the cone angle and velocity (density) is equal to −0.61 (−0.51). The correlation is even higher between the cone angle and dynamic pressure. The reason of this anticorrelation is possibly differences in solar wind on a large timescale; that is, fast and slow solar wind may correspond to slightly different average cone angles. However, a detailed study of this problem is out of scope of the paper.

The correlations between SSN and magnetospheric indices (*Kp* and *Dst*) are also higher for the last three cycles than for the whole time interval. Varying time lags, we obtain the highest correlation coefficients between SSN and *Bs* and between SSN and *Dst* for a 0-year time lag. The correlation coefficient between SSN and *Kp* peaks for 1- to 2-year time lag. In the whole interval, *Kp* better correlates with *Pdyn* and *Rsub* (with coefficients of about 0.8), while −*Dst* better correlates with *Bs* (0.71) than with *Pdyn* (0.63) or *Rsub* (−0.58).

At the same time, both *Kp* and −*Dst* nicely correlate with the IMF magnitude with correlation coefficients above 0.8. Note that we use annual average values for these correlations, and the results may differ from the correlations on shorter timescales. The correlations between solar wind parameters and magnetospheric indices were previously calculated mostly using hourly values. For example, Newell et al. (2007) obtained the correlation coefficients between *Kp* and *Bs* equal to −0.57, between *Kp* and *Pdyn* equal to 0.51, and between *Dst* and *Pdyn* equal to −0.55 (but in their study *Dst* was corrected by adding an additional term proportional to $Pdyn^{1/2}$). Lockwood et al. (2019) noted that the correlation between solar wind parameters and magnetospheric indices is higher on a longer timescale. We think that the correlations between annual solar wind and magnetospheric parameters may reveal deeper relations between them than the correlations on shorter timescale, because we eliminate any uncertainty, for example, in the time of magnetospheric response, and also remove the seasonal effects.

The *Dst* index is calculated as the deviation of the H component at midlatitude stations from their quiet day values and is supposed to depend on variations of the ring current, magnetopause current, and to a lesser extent tail current (Burton et al., 1975; see also the description of Dst at http://wdc.kugi.kyoto-u.ac.jp). An increase in the ring current decreases *Dst*, while an increase in the magnetopause current increases *Dst*. Solar wind dynamic pressure pulses may increase both the magnetopause and ring currents; however, these increases occur on different timescales. The magnetopause current rapidly increases after the pressure pulse has reached the subsolar point. The ring current reacts on a much longer timescale. First, the solar wind energy flux into the magnetosphere increases due to the magnetopause reconnection; the energy is accumulated in the magnetotail and then released through energetic particles accelerated by magnetotail reconnection. Besides, the particles are also accelerated by the convective electric field which penetrates into the magnetosphere due to the magnetopause reconnection. Considering only the annual average parameters, we cannot detect a *Dst* response to short timescale variations in the magnetopause current and mostly observe a long timescale response to the ring current. The last explains the correlation between annual *Pdyn* and −*Dst*.

The average solar wind dynamic pressure exhibits increasing trend before 1991 and decreasing trend between 1991 and 2009. It increases again in the 24th cycle until 2015. The same trends have been observed in the SSN and average IMF. Respectively, the magnetopause standoff distance increases from 9.7 to 11.6 R_E (according to the L10 model) from 1991 to 2009. Later, it decreases to 10.4 R_E in 2015 and slightly increases again. In 2017, the standoff distance is 10.6 R_E (L10 model) and 10.2 (S98 model), and in 2018 the distance in the two models increases to 10.8 and 10.4 R_E, correspondingly. These standoff distances are close to the average values in the whole 53-year interval which is equal to 10.5 R_E (L10 model) and 10.2 R_E (S98 model). Meanwhile, the extreme daily standoff distances in 2018 (in the L10 model) are equal to 8.1 and 12.8 R_E, respectively. The annual solar wind dynamic pressure decreases from 2.23 nPa in 2017 to 1.99 nPa in 2018. Note that in the three last solar minima the minimum of the dynamic pressure whether coincided with the solar minimum (between 23rd and 24th cycles) or was 2–3 years delayed (between 21st and 22nd and between 22nd and 23rd) as shown in Figure 3. Now the solar activity is nearly at minimum, and we may expect keeping about the same low-average dynamic pressure for this year.

Lockwood et al. (2009) calculated solar wind parameters during the twentieth century by reconstruction from geomagnetic activity data. They found that the solar wind velocity, IMF magnitude, and the open solar flux show a long-term increase during the first half of the twentieth century followed by peaks around 1955 and 1986 and then a decrease. They predicted the end of the current grand solar maximum between 2013 and 2027 depending on the parameter considered. This generally agrees with the trends discussed in this paper. Our annual average results (Figure) also agree with Petrinec et al. (1991) who noted that the solar wind dynamic pressure was lower in 1979–1980 than during the following solar minimum between 21st and 22nd cycles. This might be related to specific features of the 21st cycle in which a decrease of the open solar flux and solar wind speed appears right at SSN maximum in 1980 (Richardson et al., 2000). Furthermore, Dmitriev et al. (2009) concluded that the dynamic pressure anticorrelates with the SSN in the four solar cycles, from 20th to 23rd. Using the annual average values in our study, we confirm the anticorrelation between *Pdyn* and SSN in cycles 20–21 but get the correlation with the 2-year time lag in cycles 22–24. We note that even the annual magnetospheric indices (*Kp* and *Dst*) as well as the IMF magnitude display no correlation with the SSN in cycle 20. We just point out this phenomenon here but do not suggest any explanation.

Using our data set, we have found dates when the predicted subsolar magnetopause was very close to the Earth. Because of many data gaps before 1995, we find only three daily values of *Rsub* smaller than the geostationary distance 6.62 (see Table 3). In all the events, the cause of the large magnetospheric compression seems to be related to CMEs or, even, to CME series in at least two of the three events.

We suggest another way to check that the predictions of magnetopause distance with empirical models on a long timescale are reasonably good. We have compared the number of events with negative B_z at geosynchronous orbit and annual minimum magnetopause distance between 1996 and 2018. We obtain that minima in the minimum *Rsub* nearly coincide with maxima on the histogram of negative B_z events although the two plots illustrate different processes. The minimum *Rsub* corresponds to a minimum standoff distance in one event (possibly related to a strongest CME or a combination of CME-CME/CIR-CME in this year), while the number of negative B_z events may be roughly proportional to the number of most geoeffective CMEs (CME-CME or CIR-CME) in the year.

We summarize the main results below.

1. The average annual magnetopause standoff distance significantly changes during the last five solar cycles. In particular, the empirical models predict increase of the standoff distance by nearly 2 R_E from 1991 to 2009 which corresponds to a threefold decrease of the solar wind dynamic pressure. This reflects a long-term decrease of the solar activity manifested also in the annual SSN, IMF magnitude, and magnetospheric *Kp*, and *Dst* indices.
2. The annual southward IMF *Bs* correlates with SSN with a zero time lag, while the annual dynamic pressure correlates with SSN with 2- to 3-year time lag. The solar wind density poorly correlates with SSN, even taking into account the time lag; however, the density and velocity are well anticorrelated with the IMF cone angle. The density better correlates with the dynamic pressure than the velocity. The annual *Kp* better correlates with *Pdyn*, while *Dst* better correlates with *Bs*. Correspondingly, we obtain 1- to 2-year time lag for correlation between SSN and *Kp* and a zero time lag between SSN and *Dst*. The time lags correspond to the maximum of the correlation coefficients.
3. We find an anticorrelation between the annual solar wind dynamic pressure and SSN in cycles 20–21 and a correlation in cycles 22–24.
4. The annual IMF cone angle weakly correlates with SSN and does not correlate with the IMF magnitude. The annual cone angle varies from 54.0° to 61.2° with average of 57.6°.
5. We find extreme (minimal and maximal) solar wind parameters and magnetospheric indices for each year, and their variations follow the solar cycles. We suggest that the extreme solar wind parameters often result from CMEs. We show that the three events with smallest daily magnetopause distance were related to CME impacts. At least in two of the three cases two successive CMEs were observed.

The knowledge of predicted magnetopause position for the next solar cycle is important for future space missions, especially for those which are intended to observe the dayside magnetopause whether in situ or remotely. One of the forthcoming missions which will study variations of the dayside magnetopause is the Solar Wind Magnetosphere Ionosphere Link Explorer (Raab et al., 2016).

Acknowledgments
The OMNI data are available from Coordinated Data Analysis Web (CDAWeb; http://cdaweb.gsfc.nasa.gov). GOES magnetic field data are available from CDAWeb and the National Oceanic and Atmospheric Administration (NOAA; http://ngdc.noaa.gov). A. A. S. and G. B. R. acknowledge support from the U.K. Space Agency under grant ST/R002258/1. Y. V. B. was partly supported by the STFC RAL Space in-house research grant and by the NERC grant NE/P016863/1 "Space Weather Impacts on Ground-based Systems." J. S. and Z. N. acknowledge support from the Czech Science Foundation under grant 17-06065S.

References

Aellig, M. R., Lazarus, A. J., & Steinberg, J. T. (2001). The solar wind helium abundance: Variation with wind speed and the solar cycle. *Geophysical Research Letters*, *28*, 2767–2770. https://doi.org/10.1029/2000GL012771

Borovsky, J. E., & Denton, M. H. (2006). Differences between CME-driven storms and CIR-driven storms. *Journal of Geophysical Research*, *111*, A07S08. https://doi.org/10.1029/2005JA011447

Bothmer, V., & the EU-INTAS-ESA Team (2004). The solar and interplanetary causes of space storms in solar cycle 23. *IEEE Transactions on Plasma Science*, *32*(4), 1411–1414. https://doi.org/10.1109/TPS.2004.830990

Burton, R. K., McPherron, R. L., & Russell, C. T. (1975). An empirical relationship between interplanetary conditions and Dst. *Journal of Geophysical Research (1896-1977)*, *80*(31), 4204–4214. https://doi.org/10.1029/JA080i031p04204

Crooker, N. U., & Gringauz, K. I. (1993). On the low correlation between long-term averages of solar wind speed and geomagnetic activity after 1976. *Journal of Geophysical Research*, *98*(A1), 59–62. https://doi.org/10.1029/92JA01978

Denton, M. H., Borovsky, J. E., Skoug, R. M., Thomsen, M. F., Lavraud, B., Henderson, M. G., & Liemohn, M. W. (2006). Geomagnetic storms driven by ICME- and CIR-dominated solar wind. *Journal of Geophysical Research*, *111*, A07S07. https://doi.org/10.1029/2005JA011436

Dmitriev, A. V., Lin, R. L., Liu, S. Q., & Suvorova, A. V. (2016). Model prediction of geosynchronous magnetopause crossings. *Space Weather*, *14*, 530–543. https://doi.org/10.1002/2016SW001385

Dmitriev, A., Suvorova, A., & Chao, J.-K. (2011). A predictive model of geosynchronous magnetopause crossings. *Journal of Geophysical Research*, *116*, A05208. https://doi.org/10.1029/2010JA016208

Dmitriev, A. V., Suvorova, A. V., Chao, J.-K., Wang, C. B., Rastaetter, L., Panasyuk, M. I., & Myagkova, I. N. (2014). Anomalous dynamics of the extremely compressed magnetosphere during 21 January 2005 magnetic storm. *Journal of Geophysical Research: Space Physics*, *119*, 877–896. https://doi.org/10.1002/2013JA019534

Dmitriev, A. V., Suvorova, A. V., & Veselovsky, I. S. (2009). Statistical characteristics of the heliospheric plasma and magnetic field at the Earth's orbit during four solar cycles 20-23. In H. E. Johannson (Ed.), *Handbook on solar wind: Effects, dynamics and interactions* (pp. 81–144). New York: NOVA Science Publishers.

Dmitriev, A. V., Veselovsky, I. S., & Suvorova, A. V. (2005). Comparison of heliospheric conditions near the earth during four recent solar maxima. *Advances in Space Research*, *36*, 2339–2344. https://doi.org/10.1016/j.asr.2004.06.018

Dušík, v., Granko, G., Šafránková, J., Němeček, Z., & Jelínek, K. (2010). IMF cone angle control of the magnetopause location: Statistical study. *Geophysical Research Letters*, *37*, L19103. https://doi.org/10.1029/2010GL044965

Echer, E., Gonzalez, W. D., Gonzalez, A. L. C., Prestes, A., Vieira, L. E. A., dal Lago, A., & Schuch, N. J. (2004). Long-term correlation between solar and geomagnetic activity. *Journal of Atmospheric and Solar-Terrestrial Physics*, *66*, 1019–1025. https://doi.org/10.1016/j.jastp.2004.03.011

Feynman, J. (1982). Geomagnetic and solar wind cycles, 1900-1975. *Journal of Geophysical Research*, *87*, 6153–6162. https://doi.org/10.1029/JA087iA08p06153

Garner, T. W., Wolf, R. A., Spiro, R. W., Burke, W. J., Fejer, B. G., Sazykin, S., & Hairston, M. R. (2004). Magnetospheric electric fields and plasma sheet injection to low L-shells during the 4-5 June 1991 magnetic storm: Comparison between the Rice Convection Model and observations. *Journal of Geophysical Research*, *109*, A02214. https://doi.org/10.1029/2003JA010208

Gleissberg, W. (1965). The eighty-year solar cycle in auroral frequency numbers. *Journal of the British Astronomical Association*, *75*, 227–231.

Gonzalez, W. D., Gonzalez, A. L. C., & Tsurutani, B. T. (1990). Dual-peak solar cycle distribution of intense geomagnetic storms. *Planetary and Space Science*, *38*(2), 181–187. https://doi.org/10.1016/0032-0633(90)90082-2

Gopalswamy, N. (2006). Coronal mass ejections of solar cycle 23. *Journal of Astrophysics and Astronomy*, *27*(2), 243–254. https://doi.org/10.1007/BF02702527

Gopalswamy, N. (2008). Solar connections of geoeffective magnetic structures. *Journal of Atmospheric and Solar-Terrestrial Physics*, *70*, 2078–2100. https://doi.org/10.1016/j.jastp.2008.06.010

Gosling, J. T., Bame, S. J., McComas, D. J., & Phillips, J. L. (1990). Coronal mass ejections and large geomagnetic storms. *Geophysical Research Letters*, *17*(7), 901–904. https://doi.org/10.1029/GL017i007p00901

Grygorov, K., Šafránková, J., Němeček, Z., Pi, G., Přech, L., & Urbář, J. (2017). Shape of the equatorial magnetopause affected by the radial interplanetary magnetic field. *Planetary and Space Science*, *148*, 28–34. https://doi.org/10.1016/j.pss.2017.09.011

Hirshberg, J. (1973). The solar wind cycle, the sunspot cycle, and the corona. *Astrophysics and Space Science*, *20*, 473–481. https://doi.org/10.1007/BF00642216

Janardhan, P., Bisoi, S. K., Ananthakrishnan, S., Tokumaru, M., Fujiki, K., Jose, L., & Sridharan, R. (2015). A 20 year decline in solar photospheric magnetic fields: Inner-heliospheric signatures and possible implications. *Journal of Geophysical Research: Space Physics*, *120*, 5306–5317. https://doi.org/10.1002/2015JA021123

Jelínek, K., Němeček, Z., Šafránková, J., Shue, J.-H., Suvorova, A. V., & Sibeck, D. G. (2010). Thin magnetosheath as a consequence of the magnetopause deformation: THEMIS observations. *Journal of Geophysical Research*, *115*, A10203. https://doi.org/10.1029/2010JA015345

Kilpua, E. K. J., Luhmann, J. G., Jian, L. K., Russell, C. T., & Li, Y. (2014). Why have geomagnetic storms been so weak during the recent solar minimum and the rising phase of cycle 24? *Journal of Atmospheric and Solar-Terrestrial Physics*, *107*, 12–19. https://doi.org/10.1016/j.jastp.2013.11.001

King, J. H. (1979). Solar cycle variations in IMF intensity. *Journal of Geophysical Research*, *84*(A10), 5938–5940. https://doi.org/10.1029/JA084iA10p05938

Köhnlein, W. (1996). Cross-correlation of solar wind parameters with sunspots ('Long-term variations') at 1 AU during cycles 21 and 22. *Astrophysics and Space Science*, *245*(1), 81–88. https://doi.org/10.1007/BF00637804

Kuznetsov, S. N., & Suvorova, A. V. (1998). An empirical model of the magnetopause for broad ranges of solar wind pressure and B_z IMF. In J. Moen, A. Egeland, & M. Lockwood (Eds.), *Polar cap boundary phenomena* (Vol. 509, pp. 51). https://link.springer.com/book/10.1007/978-94-011-5214-3#about

Lin, R. L., Zhang, X. X., Liu, S. Q., Wang, Y. L., & Gong, J. C. (2010). A three-dimensional asymmetric magnetopause model. *Journal of Geophysical Research*, *115*, A04207. https://doi.org/10.1029/2009JA014235

Link, F. (1962). Observations et catalogue des auroras boreales apparues en occident de 626 a 1600. Geofys. Sb., 297–387.

Liu, Y. D., Hu, H., Wang, R., Yang, Z., Zhu, B., Liu, Y. A., & Richardson, J. D. (2015). Plasma and magnetic field characteristics of solar coronal mass ejections in relation to geomagnetic storm intensity and variability. *The Astrophysical Journal*, *809*(2), L34.

Lockwood, M., Bentley, S. N., Owens, M. J., Barnard, L. A., Scott, C. J., Watt, C. E., & Allanson, O. (2019). The development of a space climatology: 1. Solar wind magnetosphere coupling as a function of timescale and the effect of data gaps. *Space Weather*, *17*, 133–156. https://doi.org/10.1029/2018SW001856

Lockwood, M., Rouillard, A. P., & Finch, I. D. (2009). The rise and fall of open solar flux during the current grand solar maximum. *The Astrophysical Journal*, *700*, 937–944. https://doi.org/10.1088/0004-637X/700/2/937

Lugaz, N., Temmer, M., Wang, Y., & Farrugia, C. J. (2017). The interaction of successive coronal mass ejections: A review. *Solar Physics*, *292*(4), 64. https://doi.org/10.1007/s11207-017-1091-6

Luhmann, J. G., Lee, C. O., Li, Y., Arge, C. N., Galvin, A. B., Simunac, K., & Petrie, G. (2009). Solar wind sources in the late declining phase of cycle 23: Effects of the weak. *Solar Physics*, *256*(1), 285–305. https://doi.org/10.1007/s11207-009-9354-5

McComas, D. J., Angold, N., Elliott, H. A., Livadiotis, G., Schwadron, N. A., Skoug, R. M., & Smith, C. W. (2013). Weakest solar wind of the space age and the current "mini" solar maximum. *The Astrophysical Journal*, *779*, 2. https://doi.org/10.1088/0004-637X/779/1/2

Merka, J., Szabo, A., Šafránková, J., & Němeček, Z. (2003). Earth's bow shock and magnetopause in the case of a field-aligned upstream flow: Observation and model comparison. *Journal of Geophysical Research*, *108*(A7), 1269. https://doi.org/10.1029/2002JA009697

Němeček, Z., Šafránková, J., Lopez, R. E., Dušík, Š., Nouzák, L., Přech, L., & Shue, J.-H. (2016). Solar cycle variations of magnetopause locations. *Advances in Space Research*, *58*, 240–248. https://doi.org/10.1016/j.asr.2015.10.012

Neugebauer, M. (1981). Observations of solar-wind helium. *Fundamentals of Cosmic Physics*, *7*, 131–199.

Newell, P. T., Sotirelis, T., Liou, K., Meng, C.-I., & Rich, F. J. (2007). A nearly universal solar wind-magnetosphere coupling function inferred from 10 magnetospheric state variables. *Journal of Geophysical Research*, *112*, A01206. https://doi.org/10.1029/2006JA012015

Oh, S. Y., Yi, Y., & Kim, Y. H. (2007). Solar cycle variation of the interplanetary forward shock drivers observed at 1 AU. *Solar Physics*, *245*(2), 391–410. https://doi.org/10.1007/s11207-007-9042-2

Park, J.-S., Shue, J.-H., Kim, K.-H., Pi, G., Němeček, Z., & Šafránková, J. (2016). Global expansion of the dayside magnetopause for long-duration radial IMF events: Statistical study on GOES observation. *Journal of Geophysical Research: Space Physics*, *121*, 6480–6492. https://doi.org/10.1002/2016JA022772

Petrinec, S. M., & Russell, C. T. (1996). Near-Earth magnetotail shape and size as determined from the magnetopause flaring angle. *Journal of Geophysical Research*, *101*, 137–152. https://doi.org/10.1029/95JA02834

Petrinec, S. P., Song, P., & Russell, C. T. (1991). Solar cycle variations in the size and shape of the magnetopause. *Journal of Geophysical Research*, *96*, 7893–7896. https://doi.org/10.1029/90JA02566

Press, W. H., Teukolsky, S. A., Vetterling, W. T., & Flannery, B. P. (1992). *Numerical recipes in C*. Cambridge, UK: Cambridge University Press.

Pudovkin, M. I., Besser, B. P., & Zaitseva, S. A. (1998). Magnetopause stand-off distance in dependence on the magnetosheath and solar wind parameters. *Annales Geophysicae*, *16*, 388–396. https://doi.org/10.1007/s00585-998-0388-z

Raab, W., Branduardi-Raymont, G., Dai, L., Wang, C., Donovan, E., Enno, G., & Zheng, J. (2016). SMILE: A joint ESA/CAS mission to investigate the interaction between the solar wind and Earth's magnetosphere. Space Telescopes and Instrumentation 2016: Ultraviolet to Gamma Ray (Vol. 9905, pp. 990502). http://oro.open.ac.uk/46941/

Rank, G., Ryan, J., Debrunner, H., McConnell, M., & Schönfelder, V. (2001). Extended gamma-ray emission of the solar flares in june 1991. *Astronomy and Astrophysics*, *378*, 1046–1066. https://doi.org/10.1051/0004-6361:20011060

Richardson, I. G., Cliver, E. W., & Cane, H. V. (2000). Sources of geomagnetic activity over the solar cycle: Relative importance of coronal mass ejections, high-speed streams, and slow solar wind. *Journal of Geophysical Research*, *105*(A8), 18,203–18,213. https://doi.org/10.1029/1999JA000400

Roelof, E. C., & Sibeck, D. G. (1993). Magnetopause shape as a bivariate function of interplanetary magnetic field B_z and solar wind dynamic pressure. *Journal of Geophysical Research*, *98*, 21. https://doi.org/10.1029/93JA02362

Rouillard, A. P., Lockwood, M., & Finch, I. (2007). Centennial changes in the solar wind speed and in the open solar flux. *Journal of Geophysical Research*, *112*, A05103. https://doi.org/10.1029/2006JA012130

Samsonov, A. A., Gordeev, E., Tsyganenko, N. A., Šafránková, J., Němeček, Z., Šimunek, J., & Raeder, J. (2016). Do we know the actual magnetopause position for typical solar wind conditions? *Journal of Geophysical Research: Space Physics*, *121*, 649–6508. https://doi.org/10.1002/2016JA022471

Samsonov, A. A., Němeček, Z., Šafránková, J., & Jelínek, K. (2012). Why does the subsolar magnetopause move sunward for radial interplanetary magnetic field? *Journal of Geophysical Research*, *117*, A05221. https://doi.org/10.1029/2011JA017429

Samsonov, A. A., Sibeck, D. G., Šafránková, J., Němeček, Z., & Shue, J.-H. (2017). A method to predict magnetopause expansion in radial IMF events by MHD simulations. *Journal of Geophysical Research: Space Physics*, *122*, 3110–3126. https://doi.org/10.1002/2016JA023301

Shue, J.-H., Song, P., Russell, C. T., Steinberg, J. T., Chao, J. K., Zastenker, G., & Kawano, H. (1998). Magnetopause location under extreme solar wind conditions. *Journal of Geophysical Research*, *103*, 17,691–17,700. https://doi.org/10.1029/98JA01103

Siscoe, G. L. (1980). Evidence in the auroral record for secular solar variability. *Reviews of Geophysics and Space Physics*, *18*, 647–658. https://doi.org/10.1029/RG018i003p00647

Siscoe, G. L., Crooker, N. U., & Christopher, L. (1978). A solar cycle variation of the interplanetary magnetic field. *Solar Phys.*, *56*, 449–461. https://doi.org/10.1007/BF00152484

Suvorova, A. V., & Dmitriev, A. V. (2015). Magnetopause inflation under radial IMF: Comparison of models. *Earth and Space Science*, *2*, 107–114. https://doi.org/10.1002/2014EA000084

Suvorova, A., Dmitriev, A., Chao, J.-K., Thomsen, M., & Yang, Y.-H. (2005). Necessary conditions for geosynchronous magnetopause crossings. *Journal of Geophysical Research*, *110*, A01206. https://doi.org/10.1029/2003JA010079

Suvorova, A. V., Shue, J.-H., Dmitriev, A. V., Sibeck, D. G., McFadden, J. P., Hasegawa, H., & Němeček, Z. (2010). Magnetopause expansions for quasi-radial interplanetary magnetic field: THEMIS and Geotail observations. *Journal of Geophysical Research*, *115*, A10216. https://doi.org/10.1029/2010JA015404

Yashiro, S., Gopalswamy, N., Michalek, G., St. Cyr, O. C., Plunkett, S. P., Rich, N. B., & Howard, R. A. (2004). A catalog of white light coronal mass ejections observed by the SOHO spacecraft. *Journal of Geophysical Research*, *109*, A07105. https://doi.org/10.1029/2003JA010282

Zerbo, J.-L., Amory-Mazaudier, C., & Ouattara, F. (2013). Geomagnetism during solar cycle 23: Characteristics. *Journal of Advanced Research*, *4*, 265–274. https://doi.org/10.1016/j.jare.2012.08.010

Zerbo, J.-L., & Richardson, J. D. (2015). The solar wind during current and past solar minima and maxima. *Journal of Geophysical Research: Space Physics*, *120*, 10,250–10,256. https://doi.org/10.1002/2015JA021407